Dalton Transactions

PAPER

View Article Online
View Journal | View Issue

Cite this: *Dalton Trans.*, 2018, **47**, 4941

Intramolecular stabilization of a catalytic [FeFe]-hydrogenase mimic investigated by experiment and theory†

Indresh Kumar Pandey,[a] Mookan Natarajan,[a] Hemlata Faujdar,[a] Firasat Hussain,[a] Matthias Stein *[b] and Sandeep Kaur-Ghumaan *[a,b]

Received 21st December 2017,
Accepted 26th February 2018

DOI: 10.1039/c7dt04837h

rsc.li/dalton

The mono-substituted complex $[Fe_2(CO)_5(\mu\text{-naphthalene-2-thiolate})_2(P(PhOMe\text{-}p)_3)]$ was prepared taking after the structural principles from both [NiFe] and [FeFe]-hydrogenase enzymes. Crystal structures are reported for this complex and the all carbonyl analogue. The bridging naphthalene thiolates resemble μ-bridging cysteine amino acids. One of the naphthyl moieties forms π–π stacking interactions with the terminal bulky phosphine ligand in the crystal structure and in calculations. This interaction stabilizes the reduced and protonated forms during electrocatalytic proton reduction in the presence of acetic acid and hinders the rotation of the phosphine ligand. The intramolecular π–π stabilization, the electrochemistry and the mechanism of the hydrogen evolution reaction were investigated using computational approaches.

Introduction

Complexes of the type $\mu\text{-}S_2Fe_2(CO)_6$ were first reported in 1965 [1–3] and early chemistry for this class of complexes was developed by Seyferth and co-workers.[4–6] It was only after the report of the first crystal structure of the [FeFe]-hydrogenase active site that this class of complexes was thoroughly investigated.[7] The H-cluster has a binuclear active site with an azadithiolate bridging ligand and carbonyl and cyanide ligands to iron atoms. This [2Fe–2S] cluster unit in the active site catalyses the reversible reduction of protons to hydrogen (see Fig. 1).[8,9] Based on the structural similarity of this class of complexes to the active site a large number of organometallic [2Fe–2S] clusters have been reported as electrocatalysts for proton reduction.[10–14]

Whereas the Fe atoms of the [FeFe]-hydrogenase are connected *via* a bridging carbonyl and an azadithiolate ligand, the Ni and Fe atoms of the [NiFe]-hydrogenase enzyme are covalently bound to two bridging cysteinate amino acid residues. We here present a catalytically active homobimetallic Fe model complex mimicking the [FeFe]-enzyme with an asymmetric ligand environment and two bridging monothiolate ligands resembling the [NiFe]-enzyme (see Fig. 1).

A large number of model complexes have been reported either as structural or functional mimics of the active site.[10–15] Most of the mimics use dithiolate ligands with or without an amine group in the metal linker, see for example ref. 16–22. Only a few examples of complexes are known with monothiolate types of ligands, in which there is no covalent linkage between the two sulphur atoms.[23–25]

The consequences of removing the linker between the sulphur atoms have been investigated by Lichtenberger *et al.*

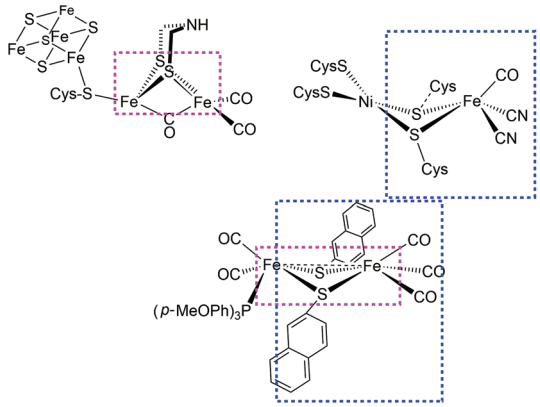

Fig. 1 Active sites ('H-cluster') of the [FeFe]-hydrogenase (top left) and the [NiFe]-hydrogenase (top right) enzymes. The $[Fe_2(CO)_5(\mu\text{-naphthalene-2-thiolate})_2(P(PhOMe\text{-}p)_3)]$ complex (below) takes up design principles from both catalytic centres.

[a]*Department of Chemistry, University of Delhi, Delhi 110007, India. E-mail: skaur@chemistry.du.ac.in*
[b]*Max-Planck-Institute for Dynamics of Complex Technical Systems, Molecular Simulations and Design Group, Sandtorstrasse 1, 39106 Magdeburg, Germany. E-mail: matthias.stein@mpi-magdeburg.mpg.de; Fax: +49-391-6110403*

† Electronic supplementary information (ESI) available: NMR spectra, X-ray data, UV-Vis, CV and additional computational results. CCDC 1054472 and 1054473. For ESI and crystallographic data in CIF or other electronic format see DOI: 10.1039/c7dt04837h

for the alkyl thiolato complex, $[Fe_2(CO)_6(\mu\text{-}SMe)_2]$ **A**.[23] Since π-electron rich polyaromatic thiolate ligands are known to influence the stability and electrochemical properties of the $[Fe_2(CO)_6]$ core, the precursor complex, $[Fe_2(CO)_6(\mu$-naphthalene-2-thiolate$)_2]$ **1** and electron rich tris(4-methoxyphenyl) phosphine (L = P(PhOMe-*p*)$_3$) were used to synthesize the diiron carbonyl complex $[Fe_2(CO)_5(\mu$-naphthalene-2-thiolate$)_2$(P(PhOMe-*p*)$_3$)] **2**. The monodentate phosphine ligand was used to provide an electron rich environment around the iron center and study its influence on the stability and electrochemical properties of **2**. The steric demand of the phosphine influences does not only affect the electronic structure of the iron atoms but also hinders the phosphine ligand rotation by forming π–π stacking interactions between the bridging monothiolate and the terminal phosphine ligand.

Results and discussion

Preparation and structural characterization

The starting complex $[Fe_2(CO)_6(\mu$-naphthalene-2-thiolato$)_2]$ **1** was synthesized as reported in the literature.[25] The synthesis of the target complex $[Fe_2(CO)_5(\mu$-naphthalene-2-thiolate$)_2$(P(PhOMe-*p*)$_3$)] **2** is presented in Scheme 1. As shown in the scheme, complex **2** was prepared by the substitution of one of the CO ligands on **1** with the electron-donating phosphine ligand (L = P(PhOMe-*p*)$_3$). A dichloromethane solution of **1** was added to an acetonitrile solution of $Me_3NO{\cdot}2H_2O$ and stirred for 10 min under an argon atmosphere at room temperature. This solution was then stirred at room temperature for 6 h under an argon atmosphere upon addition of the phosphine ligand. The complex was obtained as a blood-red solid after the removal of the solvent followed by column chromatography on a silica gel column using hexane–dichloromethane solution (3 : 2). Blood-red coloured crystals were obtained for **2** from hexane–dichloromethane solution at low temperature. The molecular structures were determined by X-ray diffraction analysis. The X-ray crystal structure of **1** not reported earlier was also obtained and is given in the ESI.†

The crystal structure of **2** is shown in Fig. 2. The crystallographic parameters are given in the ESI.† New crystallographic and structural parameters of complex **1** were available before but were determined here and are also given in the ESI.†

The Fe–Fe bond lengths for **1** and **2** are 2.49 and 2.52 Å, respectively which are close to that reported for the active site of the hydrogenase enzyme (2.6 Å).[7] The slightly elongated Fe–Fe bond is due to the stronger σ-donor properties of the phosphine ligand in **2** compared to the carbonyl group. The phosphine ligand occupies the apical position in the diiron complex **2** which is similar to that seen in the reported phosphine substituted complexes.[10,12,26–29]

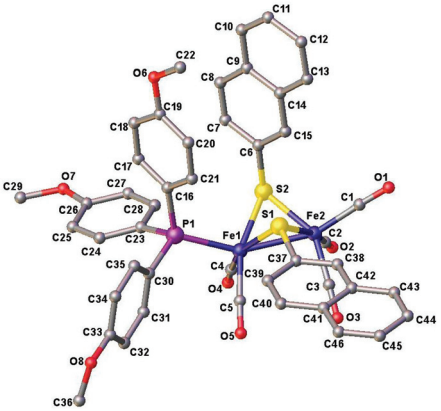

Fig. 2 Crystal structure of $[Fe_2(CO)_5(\mu$-naphthalene-2-thiolate$)_2$(P(PhOMe-*p*)$_3$)] **2**. Hydrogen atoms have been omitted for clarity. Ellipsoids are drawn at the 50% probability level.

Both complexes display a butterfly structure (Fig. 2 and ESI†) with the two naphthyl groups in an equatorial conformation in **1**. In **2** one of the *p*-PhOMe moieties of the terminal phosphine ligand leads to a spatial reorientation of one of the naphthyl rings perpendicular to the second to form π-interactions. The two naphthalene ligands thus occupy one equatorial and one rotated perpendicular axial orientation.

Complex **2** was characterized by FTIR, NMR and UV-Vis spectroscopies. The FTIR spectrum of complex **2** is shown in Fig. 3. The FTIR spectra of the mono-substituted complex **2** show several strong absorption bands in the region of 2040–1930 cm^{-1} in dichloromethane, that are assigned to terminal carbonyl groups.

The ν_{CO} bands for **2** are slightly shifted towards lower wavenumbers (by ~60 cm^{-1}) compared to **1** (2070–2000 cm^{-1}, see Table 1) but similar to those observed for analogous phosphine substituted complexes.[12,25,30] The shift towards lower wavenumbers is due to the attachment of a basic phosphine ligand to one of the iron centres. The shift is slightly more pronounced than that observed for the reported triphenyl-

Scheme 1 Synthesis of complex **2** from its precursor **1**.

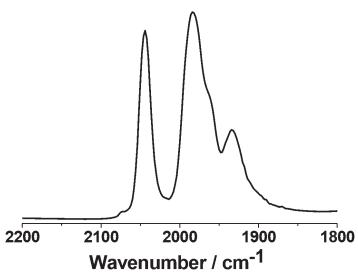

Fig. 3 FTIR spectrum of complex **2** in dichloromethane displays characteristic CO stretching frequencies from terminal carbonyl groups.

Table 1 Measured FTIR data for complexes **1** and **2** in dichloromethane

Complex	Wavenumber/cm^{-1}
1	2075, 2039, 2035, 2001
2	2044, 1984, 1960, 1934

phosphine substituted complex $[Fe_2(CO)_5(\mu\text{-naphthalene-2-thiolate})_2(PPh_3)]$.[25]

This indicates that P(PhOMe-*p*)$_3$ with the methoxy groups in the *para*-position of the phenyl rings is a stronger electron donating ligand than PPh_3. The calculated spectra for complexes **1** and **2** are given in the ESI† and allow an assignment of the FTIR bands to symmetric and asymmetric molecular stretching modes of the C═O ligands.

The ^{1}H NMR spectrum of **2** in $CDCl_3$ (see the ESI†) displayed peaks in the aromatic region (8.0–7.0 ppm) for the phenyl and naphthyl ring protons, in addition to a singlet at 3.76 ppm for the methyl protons of OMe. A singlet with a chemical shift value of 52.56 ppm was observed in ^{31}P $\{^1$H$\}$ NMR spectra which confirms the presence of the phosphine ligand. A fast rotation of the phosphine ligand around the P–Fe bond is not possible since one of the *p*-PhOMe ligands forms π-stacking interactions with one of the μ-bridging naphthylthiolates (see Fig. 2 and below) unlike the fast rotation of terminal *cis*-1,2-$C_2H_2(PPh_2)_2$ ligands in a dithiolate complex.[31]

The presence of a phosphine ligand in the mono-substituted complex **2** leads to weak metal-centered d–d transitions in the visible region and ligand-centered π–π* transitions in the UV-Vis spectra in acetonitrile and dichloromethane (see the ESI†). The appearance of the bands at a higher wavelength for **2** as opposed to those at 249 and 346 nm for the all carbonyl complex **1** is because of greater electron density at one of the iron centers due to the attachment of a phosphine ligand in the apical position.

The cyclic voltammograms (CVs) for **2** were measured in acetonitrile under an argon atmosphere. The CVs for **2** displayed two one-electron irreversible reduction waves (E_{pc} = −1.66 and −2.37 V *versus* Fc/Fc$^+$) that can be assigned $Fe^IFe^I \rightarrow Fe^IFe^0$ and $Fe^IFe^0 \rightarrow Fe^0Fe^0$ (see Fig. 4). The calculated redox

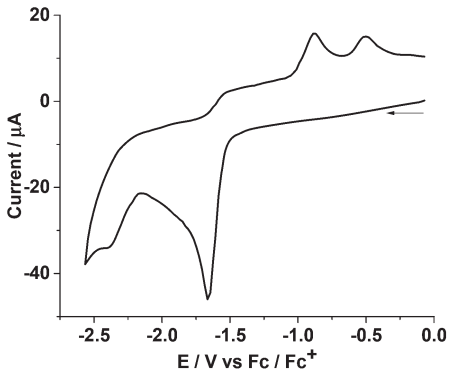

Fig. 4 Cyclic voltammogram (reduction) for complex **2** (1.2 mM) in acetonitrile at a scan rate of 0.1 V s^{-1}.

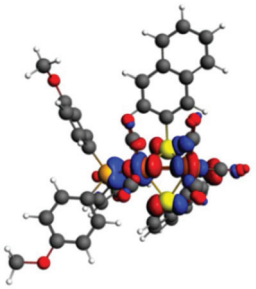

Fig. 5 The LUMO of **2** is an anti-bonding linear combination of the d_{z^2} orbitals of the iron(I) atoms. The one-electron reduction is thus going to lead to an increase of the iron–iron distance.

potentials of −1.62 V and −2.19 V support this assignment. Upon one-reduction the calculated Fe–Fe bond distance increases from 2.57 Å in **2** (2.52 Å in the crystal structure) to 2.88 Å in **2**$^-$. This can be rationalized when inspecting the LUMO of **2** which is an anti-bonding combination of the iron d_{z^2} orbitals (Fig. 5). The coordination sphere of the iron atoms remains unchanged (compared to **1**$^-$, see below). Upon one-electron reduction of complex **1**, one of the Fe–S thiolate bonds is broken (Fe···S distance 3.96 Å) and the excess electron is localized on the four-coordinate Fe only (unpaired spin density 0.95). The second reduction to yield **1**$^{2-}$ and **2**$^{2-}$ is accompanied by an increase in iron–iron bond distances to 2.75 Å and 3.54 Å, respectively, whereas the coordination sphere of **2**$^{2-}$ is unchanged, in **1**$^{2-}$ the Fe–S bond is fully dissociated (with a Fe···S distance of 4.49 Å; see the ESI† for details).

In the crystal structure of **2**, one of the aromatic phenyl rings forms π-stacking interactions with one of the bridging *S*-naphthalates (see Fig. 2 and 5).

The calculated unpaired spin density (Fig. 6) shows that in the mono-reduced Fe^IFe^0 species **2**$^-$ the electron is non-uniformly distributed over both iron atoms with atomic spin densities for $Fe(CO)_3$ of 0.25 and 0.63 for $Fe(CO)_2(P(PhOMe\text{-}p)_3)$. This is in agreement with the shifted reduction potentials of **2**/**2**$^-$ due to the strong electron donating phosphine ligand (see below).

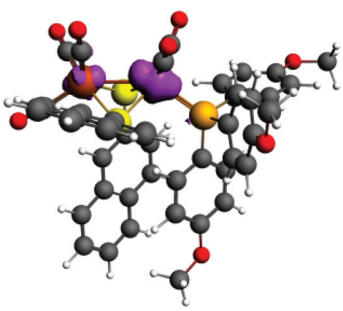

Fig. 6 Calculated spin density distribution of **2**$^-$ (Fe^IFe^0) at an isocontour value of 0.004e^-/a_0.[3]

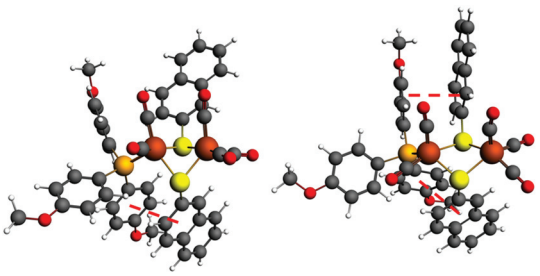

Fig. 7 Intramolecular stabilization of reduced complexes 2^- and 2^{2-} by forming π-stacking interactions between the terminal phosphine phenyl rings and the bridging μ-naphthalene-2-thiolates are indicated by red dashed lines.

In the two-fold reduced state, an additional π-stacking interaction is formed between a different aromatic ring of the terminal PhOMe-*p* substituent and the second bridging thiolate (see Fig. 7). This is accomplished by the rotation of this naphthyl ring from an equatorial into an axial orientation. This extra intramolecular interaction helps to stabilize 2^{2-} and retain the coordination environment.

Two one-electron irreversible oxidations were also observed at E_{pa} = 0.29 and 1.00 V *versus* Fc/Fc^+ which might be ascribed as $Fe^IFe^I \rightarrow Fe^IFe^{II}$ and $Fe^IFe^{II} \rightarrow Fe^{II}Fe^{II}$, respectively (see the ESI†). The assignment of one-electron oxidation events is supported by calculations in which BP86 performs superior to B3LYP (see Table 2). The reduction of compound **2** occurs at a more negative potential than **1** and its oxidation at a less positive potential than complex **1** (Table 2).[25]

This is due to the substitution of CO for $P(PhOMe\text{-}p)_3$ making the [Fe–Fe] center of **2** more electron-rich than **1**. The electrochemical data are consistent with the results of similar model complexes reported in the literature.[26] Furthermore, the reduction potentials for **2** are slightly more negative in comparison with that of $[Fe_2(CO)_5(\mu\text{-naphthalene-2-thiolate})_2(PPh_3)]$ **B** thus, indicating better electron donating properties of the phosphine ligand in **2** (Table 2).

Table 2 Experimental and calculated electrochemical data of complexes **1** and **2** and comparison with the literature

Complex	E_{pc}/V	E_{pa}/V	E_{cat}/V	Overpotential/V
Exp. 1	−1.33	0.61	−2.00	−0.54
Calc.	**1/1$^-$**			
BP86	−1.41			
B3LYP	−1.66			
Exp. 2	−1.66	0.29	−2.02	−0.56
Calc.	**2/2$^-$**	**2/2$^+$**		
BP86	−1.62	0.42		
B3LYP	−1.76	0.43		
Exp.	−2.37	1.00		
Calc.	**2$^-$/2^{2-}**	**2$^+$/2^{2+}**		
BP86	−2.19	0.91		
B3LYP	−2.95	0.73		
B [26]	−1.49	0.31	−1.97	−0.51
C [25]	−1.44	0.81	−2.26	−0.80

Upon oxidation of **2** to 2^+ and 2^{2+}, the Fe^IFe^{II} and $Fe^{II}Fe^{II}$ states preserve their structural integrity. All covalent bonds remain intact. Complex **2** was examined for its ability to act as an electrocatalyst for the reduction of protons to molecular hydrogen in the presence of acetic acid (Fig. 8). The complex was found to be unstable in the presence of stronger acids (perchloric acid). CVs of **2** in the presence of acetic acid show a new peak at −2.02 V *versus* Fc/Fc^+ which shifts cathodically with an increase in the amount of acid. The increase of current at this reduction potential with an increase in the amount of acid can be attributed to the reduction of protons to molecular hydrogen.[26] The first reduction peak at −1.66 V observed in the absence of an acid is shifted anodically to −1.60 V upon addition of acid without much increase in current with increasing amounts of acid.

The diiron-based HER catalysts operate *via* an intermediate mixed-valence hydride species considered to be a rare class of complex[10,32] and difficult to isolate.[12] After reduction to 2^- (see Fig. 5), such a hydride species is obtained from the first protonation in an ECEC mechanism. One-electron reduction of mono-[33,34] and diiron-complexes[35] with bridging dithiolates usually leads to an elongation of one Fe–S bond to afford initial protonation of the μ_1-thiolate. In the presence of a second coordination shell basic site[36,37] an initial ligand protonation might be kinetically driven but eventually a thermodynamically favoured metal–hydride species is subsequently formed.[37]

Both BP86 and B3LYP calculations were shown to yield proton affinities within 1–2 kcal mol^{-1} with respect to CCSD(T) calculations and experiments.[38] BP86 slightly overestimates and B3LYP slightly under-estimates proton affinities. In the absence of a ligand protonation site (such as nitrogen), 2^- can be protonated to yield either a terminal Fe–hydride (proton affinity of 8 kcal mol^{-1}) or a μ-bridging hydride (proton affinity of 17 kcal mol^{-1}) (complex **2H**, see Table 3). A terminal iron–hydride can be thermodynamically unstable and convert to the bridging hydride by an intramolecular isomerization even at

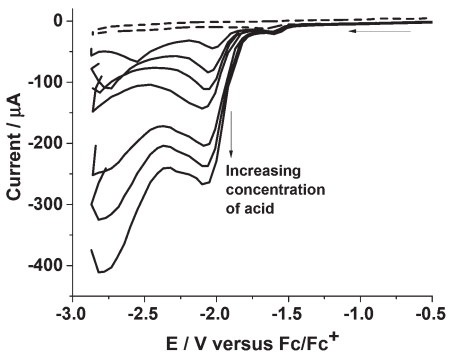

Fig. 8 Cyclic voltammograms for complex **2** (1.2 mM) in acetonitrile without acid (------) and with increasing amounts (5.79, 11.56, 17.31, 23.05, 34.46, and 62.65 mM) of acetic acid (—) at a scan rate of 0.1 V s^{-1}.

Table 3 Computed differences in proton affinities for 2^- to afford **2H**. Gibbs free energy differences between the terminal $\mathbf{2H_{terminal}}$ and bridging $\mathbf{2H_{bridging}}$ hydrides are given in kcal mol^{-1}. Systematic errors are thus expected to cancel out. A positive value indicates a preference for a μ-hydride

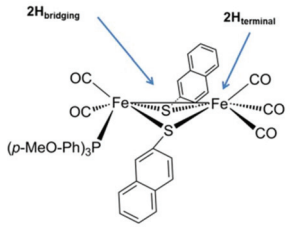

2^-/**2H**	BP86	BP86-COSMO	B3LYP	B3LYP-COSMO
	+8.4	+8.7	+2.6	+3.4

low temperature.[39] In the absence of a vacant terminal protonation site, a 'rotated' structure with a semi-bridging CO ligand is obtained for $\mathbf{2H_{terminal}}$, which is also observed for related dithiolate complexes.[40] The equilibrium between 'rotated' and 'unrotated' structures is mediated by subtle steric effects of bidentate dithiolate ligands (ethanedithiolate *versus* propanedithiolate).[42]

Protonation of a bridging naphthalenethiolate is less favoured with a calculated proton affinity of ~3 kcal mol^{-1} which is also found in ref. 41. The protonated thiolate might also re-arrange to a terminal iron hydride. Protonation of one of the μ_2-naphthalenethiolates might be the reason for the catalyst instability and degradation in strong acids (perchloric acid).

In the plot of i_{cat}/i_p *versus* acid concentration for complex **2**, the current first increases and then levels off at a maximum of 62.65 mM of acid in solution (see the ESI†). The initial linearity indicates that the reaction is second order with respect to acid concentration (see eqn (1)) for a scan rate of 0.1 V s^{-1} (see the ESI†).

$$\frac{i_{cat}}{i_p} = \frac{n}{0.4463} \cdot \sqrt{\frac{RT(k[H^+]^x)}{F\nu}} \quad (1)$$

Also, the ratio i_{cat}/i_p for two different acetic acid concentrations (20.8 and 62 mM) varies linearly with the square root of the scan rate ($\nu^{-1/2}$) confirming the validity of eqn (1) (see the ESI†). Scan rate independence is achieved only at a scan rate of 0.4 V s^{-1} and greater (see the ESI†). The plot of the amount of acetic acid *versus* k_{obs} (turnover frequency (TOF) from eqn (2) and (3)) for complex **2** calculated from the i_{cat}/i_p ratio is shown in Fig. 9.

$$k_{obs} = k[H^+]^x \quad (2)$$

$$k_{obs} = 1.94\nu\left(\frac{i_{cat}}{i_p}\right)^2 \quad (3)$$

A value of i_{cat}/i_p of 21.43 was obtained for **2** (1.62 mM) for the highest acid concentration investigated (62.65 mM), corresponding to a turnover frequency of 88 s^{-1}.[42] The TOF of **2** was determined by taking the successive cyclic voltammograms of the reaction mixtures for which the concentration of acetic acid was systematically increased until the k_{obs} (TOF) remained constant. For comparison, the data generated for complexes **1**, **B** and $[Fe_2(CO)_6(\mu\text{-SPh})_2]$ **C** have also been included (see the ESI†).[24,25] Furthermore, the catalytic efficiency was examined by determining the overpotential in MeCN. The overpotential for **2**, calculated as described by Evans *et al.*, was found to be −0.56 V (Table 2).[26] Complex **2** was found to be a better catalyst in comparison with complexes **1**, **B** and **C**. Also, complex **2** catalyzes the reduction of protons at a slightly more negative potential than **1** and **B** and at a less negative potential than **C**.

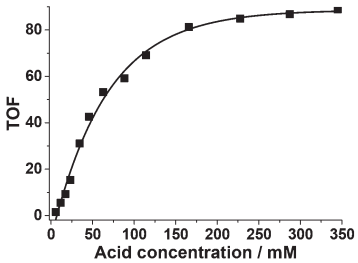

Fig. 9 Dependence of TOF for **2** (1.62 mM) upon acetic acid concentration in 0.1 M *n*-Bu_4NPF_6/MeCN at a scan rate of 0.1 V s^{-1}.

The background current due to the direct reduction of protons at the glassy carbon electrode without the catalyst in the presence of acetic acid was found to be negligible for potentials in the range of −1.4 to −2.1 V. Hence, the acid-induced currents in the presence of catalysts can be attributed to catalytic turnover. Similar background measurements for different acids in the absence of a catalyst have also been recently looked into by McCarthy *et al.*[43]

The second one electron reduction from **2H** to $\mathbf{2H^-}$ was calculated to occur at redox potentials of −1.67 V/−1.98 V (BP86/B3LYP) for $\mathbf{2H_{bridging}}$ compared to −2.19 V for $\mathbf{2}^-/\mathbf{2}^{2-}$ reduction of the sole catalyst in the absence of an acid. The final chemical (C) protonation step from $\mathbf{2H^-}$ to **2HH** is unlikely to occur at an iron atom since a dihydride species in a formal Fe^IFe^I complex would be formed. The metal oxidation state can be preserved when protonation occurs at a sulfur atom of the bridging μ-thionaphthalate. Such a protonation is thermodynamically feasible with a calculated proton affinity of 19 kcal mol^{-1} (BP86) and 25 kcal mol^{-1} (B3LYP). This ECEC step, however, leads to a *cul-de-sac* since the doubly reduced species displays two π–π stacking interactions between the bridging μ-thiolates and the terminal P(PhOMe-*p*) ligands (see Fig. 7 and Fig. 10). This interaction hinders the intramolecular rotational isomerization of the sterically demanding μ-naphthalene around the S–C carbon which would be necessary to bring the protonated sulfur and the bridging hydride in close spatial vicinity.

The monothiolate bridging ligands, unlike bridging dithiolates, enable a direct protonation of the μ-hydride species to form a Fe^0–H_2–Fe^0 complex. Such a protonation retains the

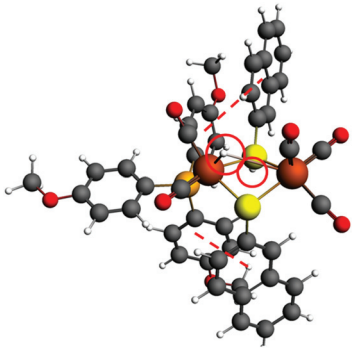

Fig. 10 The **2HH** species with (i) a μ-bridging hydride and (ii) a protonated naphthalene-thiolate after two one electron reductions. The two protons added are circled in red. π–π stacking interactions between bridging naphthalene ligands and terminal phenyl rings are indicated as dashed lines. This stabilization hinders an intramolecular isomerization required to release molecular hydrogen.

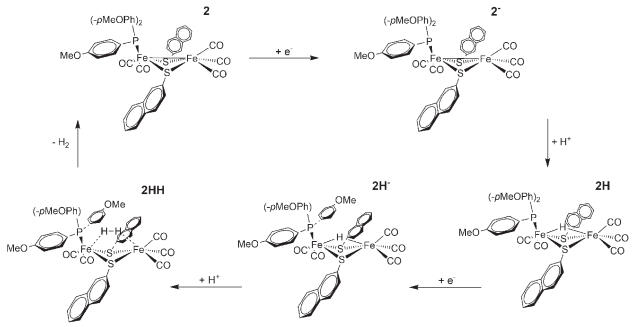

Scheme 2 Suggested mechanism for the electrocatalytic proton reduction of complex **2** (see the text for details).

metal oxidation states to **2HH** from which molecular hydrogen is easily released and complex **2** is recovered (see Scheme 2). During the path of the electrocatalytic proton reduction, the Fe···Fe distances only change by less than 0.8 Å (see the ESI†). The suggested mechanism resembles the reverse reaction of a [NiFe]-hydrogenase enzyme when oxidizing H_2. Molecular hydrogen is activated between the Ni and Fe atoms of the active site and a μ-hydride is obtained as a stable intermediate Ni–C.

Conclusions

A new diiron carbonyl complex $[Fe_2(CO)_5$(μ-naphthalene-2-thiolate$)_2$(P(PhOMe-*p*$)_3$)] **2** was prepared from $[Fe_2(CO)_6$(μ-naphthalene-2-thiolate$)_2$] **1** using the monodentate phosphine ligand, P(PhOMe-*p*$)_3$ and characterized by different spectroscopic techniques. The crystal structures for both complexes **1** and **2** are reported. The electrochemical investigations of complex **2** were performed in acetonitrile in the presence of acetic acid. Complex **2** was found to successfully electro-catalyze the reduction of acetic acid to H_2 with an overpotential of −0.56 V. This value of overpotential is towards the lower side in comparison with similar other reported complexes.[25,26,44,45]

The bridging monothiolates in **2** resemble the bridging cysteine motif in [NiFe]-hydrogenase enzymes (see Fig. 1). Their rotational flexibility is limited due to the interactions with the protein matrix. In the model complex, this is accomplished by intramolecular stabilization. The monothiolates in the enzyme and in the model complex are sufficiently small to allow a direct protonation of the metal–metal bond to form a μ-hydride species.[46,47] This is not possible in the case of[FeFe]-hydrogenase enzymes. In [FeFe] model complexes with bidentate thiolate ligands, a terminal hydride is formed initially which requires an intramolecular isomerization to form the bridging hydride. Such a re-orientation is not feasible in the [FeFe] enzyme since the terminal inorganic ligands form strong hydrogen bonds with the surrounding amino acid residue.[48]

The monothiolate-bridged [FeFe] complex **2** is remarkably stable and can be reduced and oxidized two times without any structural distortion or degradation. This is accomplished by a combination of sufficient molecular flexibility from monothiolate bridging ligands and an electron rich and sterically demanding terminal P(PhOMe-*p*$)_3$ ligand which forms hydrophobic interactions with naphthalene-thiolates.

Previous attempts to stabilize hydrogen evolving catalysts have mainly focused on the covalent fixation of small molecules on electrode surfaces[49,50] incorporating into metal–organic frameworks[51] or hydrogel films[52] to improve the number of catalytic turnovers and the long-term catalyst stability. The concept of introducing stabilizing hydrophobic π–π interactions by incorporating both aromatic μ-bridging monothiolate ligands with a sufficient degree of rotational flexibility and terminal ligands with aromatic substituents has not been explored before. These apparently weak π–π interactions are sufficient to afford a compromise between structural flexibility of the catalyst and the integrity and stability of the coordination environment. Due to the hydrophobic nature of the π-interactions these are also expected to hold in aqueous media.

Experimental

Methods and materials

All the experiments were carried out under an inert atmosphere using Schlenk techniques unless otherwise specified. Complex $[Fe_2(CO)_6$(μ-naphthalene-2-thiolate$)_2$] **1** was prepared according to the reported procedure.[25] All the anhydrous solvents (dichloromethane, acetonitrile and toluene) and starting materials were obtained from Sigma-Aldrich and used without further purification. The deuterated solvents were also obtained from Sigma-Aldrich. The ^{1}H and ^{31}P NMR spectra were recorded at room temperature in $CDCl_3$ solution with a JEOL 400 MHz NMR Spectrometer. FTIR spectra were recorded from dichloromethane solutions of the samples over the range of 400–4000 cm^{-1} on a Perkin Elmer FTIR Spectrometer. The UV-Vis spectra for complex **1** were recorded on a PerkinElmer

Lambda-25 spectrophotometer and for complex **2** on an Avantes Avaspec-2048-USB2. The elemental analyses were carried out with a Vario Micro Cube elemental analyzer.

Synthesis of [$Fe_2(CO)_5$(μ-naphthalene-2-thiolate)(P(PhOMe-*p*)$_3$)]

A dichloromethane solution of **1** (200 mg, 0.334 mmol, 15 mL) was added to an acetonitrile solution of trimethylamine *N*-oxide dihydrate ($Me_3NO{\cdot}2H_2O$) (37.1 mg, 0.334 mmol, 15 mL) and stirred for 10 min under an argon atmosphere. This was followed by the addition of tris(4-methoxyphenyl) phosphine (118 mg, 0.334 mmol) dissolved in 5 mL of CH_2Cl_2. The solution was stirred at room temperature for 6 h and the solvent was removed by using a rotary evaporator. The residue was chromatographed on a silica gel column. Elution with a mixture of hexane/dichloromethane (3 : 2) afforded a red coloured solution. Complex **2** was obtained as an air-stable blood-red powder after the removal of solvent. The complex was then recrystallized from hexane/CH_2Cl_2 by a layering method at −10 °C.

Yield: 154.1 mg (50%). FTIR (cm^{-1}, CH_2Cl_2): (ν_{CO}) 2044, 1984, 1960, 1934. FTIR (cm^{-1}, CH_3CN): (ν_{CO}) 2042, 1981, 1960, 1932. ^{1}H NMR (400 MHz, $CDCl_3$): δ = 7.72–7.48 (m), 7.15–7.06 (m) ppm, 6.84 (m), 3.76 (s, 9H, OMe) ppm. ^{13}C NMR (400 MHz, $CDCl_3$): 210 (CO), 161 (Ph), 140–135 (naphthyl), 55.5 (Me) ppm. ^{31}P NMR (161.83 MHz, $CDCl_3$): δ = 52.6 (s) ppm. Anal. calcd for $C_{46}H_{35}Fe_2O_8PS_2$: C, 59.89; H, 3.82. Found: C, 59.46; H, 3.41.

X-ray crystallography

Single crystals of **1** and **2** were grown by slow evaporation of hexane/dichloromethane solutions at low temperature. X-Ray data of **1** and **2** were collected on an Oxford X-Calibur-S single crystal X-ray diffractometer using Mo-K_α radiation. Significant crystallographic parameters and refinement details are listed in the ESI.† The structures were solved and refined by full-matrix least-squares techniques on F^2 using the SHELX-97 (SHELXTL program package).[53] CCDC reference numbers 1054472 (**2**) and 1054473 (**1**)† contain the supplementary crystallographic data for this paper.

Electrochemistry

Electrochemical measurements were conducted in acetonitrile with 0.1 M tetrabutylammoniumhexafluorophosphate (Sigma-Aldrich, electrochemical grade) as the supporting electrolyte that was dried in a vacuum at 383 K. Cyclic voltammetry was carried out using an Autolab potentiostat with a GPES electrochemical interface (Eco Chemie). The working electrode was a glassy carbon disc (diameter 3 mm, freshly polished) for cyclic voltammetry. Platinum was used as the counter electrode. The reference electrode was a non-aqueous Ag/Ag^+ electrode (CH Instruments, 0.010 M $AgNO_3$ in acetonitrile). All the potentials are quoted against the ferrocene–ferrocenium couple (Fc/Fc^+); ferrocene was added as an internal standard at the end of the experiments. All solutions were prepared from dry acetonitrile (Sigma-Aldrich, spectroscopic grade, dried with molecular sieves 3 Å).

Computational details

ADF2016[54,55] was used with the BP86[56,57] and B3LYP[58,59] exchange–correlation functionals, Grimme's dispersion correction with Becke–Johnson damping[60] and a TZP Slater-type basis set for all atoms. The solvent (acetonitrile) was used in a COSMO solvation model[61,62] using the Klamt atomic radii and surface definition with corrections for outlying charges. Thermodynamic corrections were obtained using statistical thermodynamics from BP86 calculations under standard conditions.[63] Redox potentials were calculated following ref. 64 and are given relative to a Fc/Fc^+ reference electrode in acetonitrile (calculated absolute potentials are 4.94 V for BP86 and 5.18 V for B3LYP). The BP86 value agrees well with the experiment (4.98 V (ref. 65)).

Conflicts of interest

There are no conflicts to declare.

Acknowledgements

Financial support from the Department of Science & Technology (DST), India (SR/S1/IC-28/2011) and the Max Planck Society for the Advancement of Science is gratefully acknowledged. This work was in part funded by the COST Action CM1305 'ECOSTBio'. SKG is thankful to the University of Delhi, India for providing a R&D grant and to DST and Max Planck Society for the Max Planck-India Visiting Fellowship. IKP and HF are grateful to UGC and MN is grateful to the CSIR for a Research Fellowship. Open Access funding was provided by the Max Planck Society.

References

1 C. H. Wei and L. F. Dahl, *Inorg. Chem.*, 1965, **4**, 1–11.
2 L. J. Farrugia, C. Evans, H. M. Senn, M. M. Hänninen and R. Sillanpää, *Organometallics*, 2012, **31**, 2559–2570.
3 I. L. Eremenko, H. Berke, A. A. H. van der Zeijden, B. I. Kolobkov and V. M. Novotortsev, *J. Organomet. Chem.*, 1994, **471**, 123–132.
4 D. Seyferth, R. S. Henderson and M. K. Gallagher, *J. Organomet. Chem.*, 1980, **193**, C75–C78.
5 (*a*) D. Seyferth, L.-C. Song and R. S. Henderson, *J. Am. Chem. Soc.*, 1981, **103**, 5103–5107; (*b*) D. Seyferth, R. S. Henderson and L. C. Song, *Organometallics*, 1982, **1**, 125–133.
6 D. Seyferth, R. S. Henderson, L.-C. Song and G. B. Womack, *J. Organomet. Chem.*, 1985, **292**, 9–17.
7 J. W. Peters, W. N. Lanzilotta, B. J. Lemon and L. C. Seefeldt, *Science*, 1998, **282**, 1853–1858.
8 Y. Nicolet, C. Piras, P. Legrand, C. E. Hatchikian and J. C. Fontecilla-Camps, *Structure*, 1999, **7**, 13–23.

9 Y. Nicolet, A. L. de Lacey, X. Vernande, V. M. Fernandez, E. C. Hatchikian and J. C. Fontecilla-Camps, *J. Am. Chem. Soc.*, 2001, **123**, 1596–1601.
10 C. Tard and C. J. Pickett, *Chem. Rev.*, 2009, **109**, 2245–2274.
11 W. Lubitz, H. Ogata, O. Rüdiger and E. Reijerse, *Chem. Rev.*, 2014, **114**, 4081–4148.
12 N. Wang, M. Wang, L. Chen and L. Sun, *Dalton Trans.*, 2013, **42**, 12059–12071.
13 J. A. Wright and C. J. Pickett, *ChemCatChem*, 2012, **4**, 1723–1724.
14 I. K. Pandey, M. Natarajan and S. Kaur-Ghumaan, *J. Inorg. Biochem.*, 2015, **143**, 88–110.
15 S. Kaur-Ghumaan and M. Stein, *Dalton Trans.*, 2014, **43**, 9392–9405.
16 B. E. Barton, M. T. Olsen and T. B. Rauchfuss, *J. Am. Chem. Soc.*, 2008, **130**, 16834–16835.
17 S. J. Borg, T. Behrsing, S. P. Best, M. Razavet, X. M. Liu and C. J. Pickett, *J. Am. Chem. Soc.*, 2004, **126**, 16988–16999.
18 S. Ezzaher, J. F. Capon, F. Gloaguen, F. Y. Petillon, P. Schollhammer and J. Talarmin, *Inorg. Chem.*, 2007, **46**, 9863–9872.
19 F. Gloaguen, J. D. Lawrence, M. Schmidt, S. R. Wilson and T. B. Rauchfuss, *J. Am. Chem. Soc.*, 2001, **123**, 12518–12527.
20 A. K. Justice, T. B. Rauchfuss and S. R. Wilson, *Angew. Chem., Int. Ed.*, 2007, **46**, 6152–6154.
21 A. Le Cloirec, S. C. Davies, D. J. Evans, D. L. Hughes, C. J. Pickett, S. P. Best and S. Borg, *Chem. Commun.*, 1999, 2285–2286.
22 D. Schilter, M. J. Nilges, M. Chakrabarti, P. A. Lindahl, T. B. Rauchfuss and M. Stein, *Inorg. Chem.*, 2012, **51**, 2338–2348.
23 O. In-noi, K. J. Haller, G. B. Hall, W. P. Brezinski, J. M. Marx, T. Sakamoto, D. H. Evans, R. S. Glass and D. L. Lichtenberger, *Organometallics*, 2014, **33**, 5009–5019.
24 Y. Si, M. Hu and C. Chen, *C. R. Chim.*, 2008, **11**, 932–937.
25 C. A. Mebi, D. S. Karr and B. C. Noll, *Polyhedron*, 2013, **50**, 164–168.
26 G. A. N. Felton, C. A. Mebi, B. J. Petro, A. K. Vannucci, D. H. Evans, R. S. Glass and D. L. Lichtenberger, *J. Organomet. Chem.*, 2009, **694**, 2681–2699.
27 D. M. Heinekey, *J. Organomet. Chem.*, 2009, **694**, 2671–2680.
28 J. F. Capon, F. Gloaguen, F. Y. Petillon, P. Schollhammer and J. Talarmin, *C. R. Chim.*, 2008, **11**, 842–851.
29 J. F. Capon, F. Gloaguen, F. Y. Petillon, P. Schollhammer and J. Talarmin, *Coord. Chem. Rev.*, 2009, **253**, 1476–1494.
30 J. A. Cabeza, M. A. Martínez-García, V. Riera, D. Ardura and S. García-Granda, *Organometallics*, 1998, **17**, 1471–1477.
31 W. Wang, M. J. Nilges, T. B. Rauchfuss and M. Stein, *J. Am. Chem. Soc.*, 2013, **135**, 3633–3639.
32 M. Wang, L. Chen and L. Sun, *Energy Environ. Sci.*, 2012, **5**, 6763–6778.
33 S. Kaur-Ghumaan, L. Schwartz, R. Lomoth, M. Stein and S. Ott, *Angew. Chem., Int. Ed.*, 2010, **49**, 8033–8036.
34 M. Natarajan, H. Faujdar, S. M. Mobin, M. Stein and S. Kaur-Ghumaan, *Dalton Trans.*, 2017, **46**, 10050–10056.
35 P. S. Singh, H. C. Rudbeck, P. Huang, S. Ezzaher, L. Eriksson, M. Stein, S. Ott and R. Lomoth, *Inorg. Chem.*, 2009, **48**, 10883–10885.
36 A. Orthaber, M. Karnahl, S. Tschierlei, D. Streich, M. Stein and S. Ott, *Dalton Trans.*, 2014, **43**, 4537–4549.
37 G. Eilers, L. Schwartz, M. Stein, G. Zampella, L. de Gioia, S. Ott and R. Lomoth, *Chem. – Eur. J.*, 2007, **13**, 7075–7084.
38 M. Swart, E. Rosler and F. M. Bickelhaupt, *J. Comput. Chem.*, 2006, **27**, 1486–1493.
39 B. E. Barton, G. Zampella, A. K. Justice, L. De Gioia, T. B. Rauchfuss and S. R. Wilson, *Dalton Trans.*, 2010, **39**, 3011–3019.
40 E. J. Lyon, I. P. Georgakaki, J. H. Reibenspies and M. Y. Darensbourg, *J. Am. Chem. Soc.*, 2001, **123**, 3268–3278.
41 R. Zaffaroni, T. B. Rauchfuss, D. L. Gray, L. De Gioia and G. Zampella, *J. Am. Chem. Soc.*, 2012, **134**, 19260–19269.
42 (*a*) V. Artero and J.-M. Savéant, *Energy Environ. Sci.*, 2014, **7**, 3808–3814; (*b*) C. Costentin, G. Passard and J.-M. Savéant, *J. Am. Chem. Soc.*, 2015, **137**, 5461–5467.
43 B. D. McCarthy, D. J. Martin, E. S. Rountree, A. C. Ullman and J. L. Dempsey, *Inorg. Chem.*, 2014, **53**, 8350–8361.
44 R. J. Wright, C. Lim and T. D. Tilley, *Chem. – Eur. J.*, 2009, **15**, 8518–8525.
45 A. L. Haley, L. N. Broadbent, L. S. McDaniel, S. T. Heckman, C. H. Hinkle, N. N. Gerasimchuk, J. C. Hershberger and C. A. Mebi, *Polyhedron*, 2016, **114**, 218–224.
46 M. Stein and W. Lubitz, *Phys. Chem. Chem. Phys.*, 2001, **3**, 2668–2675.
47 M. Stein and W. Lubitz, *Curr. Opin. Chem. Biol.*, 2002, **6**, 243–249.
48 A. R. Finkelmann, M. T. Stiebritz and M. Reiher, *Chem. Sci.*, 2014, **5**, 215–221.
49 P. Rodriguez-Macia, N. Priyadarshani, A. Dutta, C. Weidenthaler, W. Lubitz, W. J. Shaw and O. Rudiger, *Electroanalysis*, 2016, **28**, 2452–2458.
50 P. Rodriguez-Macia, A. Dutta, W. Lubitz, W. J. Shaw and O. Rudiger, *Angew. Chem., Int. Ed.*, 2015, **54**, 12303–12307.
51 S. Pullen, H. H. Fei, A. Orthaber, S. M. Cohen and S. Ott, *J. Am. Chem. Soc.*, 2013, **135**, 16997–17003.
52 V. Fourmond, S. Stapf, H. G. Li, D. Buesen and J. Birrell, *J. Am. Chem. Soc.*, 2015, **137**, 5494–5505.
53 G. M. Sheldrick, *SHELX-97 Program for Crystal Structure Solution Refinement*, University of Gottingen, Gottingen, Germany, 1997.
54 E. J. Baerends, T. Ziegler, A. J. Atkins, J. Autschbach, O. Baseggio, *et al.*, *SCM, Theoretical Chemistry*, Vrije Universiteit, Amsterdam, The Netherlands, 2016.
55 G. te Velde, F. M. Bickelhaupt, E. J. Baerends, C. F. Guerra, S. J. A. Van Gisbergen, J. G. Snijders and T. Ziegler, *J. Comput. Chem.*, 2001, **22**, 931–967.
56 A. D. Becke, *Phys. Rev. A*, 1988, **38**, 3098–3100.
57 J. P. Perdew and W. Yue, *Phys. Rev. B: Condens. Matter Mater. Phys.*, 1986, **33**, 8800–8802.
58 A. D. Becke, *J. Chem. Phys.*, 1993, **98**, 1372–1377.
59 P. J. Stephens, F. J. Devlin, C. F. Chabalowski and M. J. Frisch, *J. Phys. Chem.*, 1994, **98**, 11623–11627.

60 S. Grimme, S. Ehrlich and L. Goerigk, *J. Comput. Chem.*, 2011, **32**, 1456–1465.
61 A. Klamt and G. Schuurmann, *J. Chem. Soc., Perkin Trans. 2*, 1993, 799–805.
62 C. C. Pye and T. Ziegler, *Theor. Chem. Acc.*, 1999, **101**, 396–408.
63 D. A. McQuarrie and J. D. Simon, *Molecular Thermodynamics*, University Science Books, Sausalito, 1991.
64 (*a*) A. V. Marenich, J. Ho, M. L. Coote, C. J. Cramer and D. J. Truhlar, *Phys. Chem. Chem. Phys.*, 2014, **16**, 15068–15106; (*b*) M. Namazian, C. Y. Lin and M. L. Coote, *J. Chem. Theory Comput.*, 2010, **6**, 2721–2725; (*c*) A. V. Marenich, J. M. Ho, M. L. Coote, C. J. Cramer and D. G. Truhlar, *Phys. Chem. Chem. Phys.*, 2014, **16**, 15068–15106.
65 V. V. Pavlishchuk and A. W. Addison, *Inorg. Chim. Acta*, 2000, **298**, 97–102.